Cell Reports
Resource

In Vivo Visualization of Subtle, Transient, and Local Activity of Astrocytes Using an Ultrasensitive Ca^{2+} Indicator

Kazunori Kanemaru,[1,9] Hiroshi Sekiya,[1,9] Ming Xu,[2] Kaname Satoh,[1] Nami Kitajima,[1] Keitaro Yoshida,[2] Yohei Okubo,[1] Takuya Sasaki,[3] Satoru Moritoh,[4] Hidetoshi Hasuwa,[5] Masaru Mimura,[2] Kazuki Horikawa,[6] Ko Matsui,[7] Takeharu Nagai,[8] Masamitsu Iino,[1,*] and Kenji F. Tanaka[2,*]

[1]Department of Pharmacology, Graduate School of Medicine, The University of Tokyo, Bunkyo, Tokyo 113-0033, Japan
[2]Department of Neuropsychiatry, School of Medicine, Keio University, Shinjuku, Tokyo 160-8582, Japan
[3]Neurobiology Section and Center for Neural Circuits and Behavior, Division of Biological Sciences, University of California, San Diego, San Diego, CA, 92093-0357, USA
[4]Department of Ophthalmology, Tohoku University Graduate School of Medicine, Sendai 980-8574, Japan
[5]Genome Information Research Center, Osaka University, Suita 565-0871, Japan
[6]Support Center for Advanced Medical Sciences, Institute of Health Biosciences, The University of Tokushima Graduate School, Tokushima 770-8503, Japan
[7]Division of Interdisciplinary Medical Science, Center for Neuroscience, Tohoku University Graduate School of Medicine, Sendai 980-8575, Japan
[8]The Institute of Scientific and Industrial Research, Osaka University, Ibaraki 567-0047, Japan
[9]Co-first author
*Correspondence: iino@m.u-tokyo.ac.jp (M.I.), kftanaka@a8.keio.jp (K.F.T.)
http://dx.doi.org/10.1016/j.celrep.2014.05.056

SUMMARY

Astrocytes generate local calcium (Ca^{2+}) signals that are thought to regulate their functions. Visualization of these signals in the intact brain requires an imaging method with high spatiotemporal resolution. Here, we describe such a method using transgenic mice expressing the ultrasensitive ratiometric Ca^{2+} indicator yellow Cameleon-Nano 50 (YC-Nano50) in astrocytes. In these mice, we detected a unique pattern of Ca^{2+} signals. These occur spontaneously, predominantly in astrocytic fine processes, but not the cell body. Upon sensory stimulation, astrocytes initially responded with Ca^{2+} signals at fine processes, which then propagated to the cell body. These observations suggest that astrocytic fine processes function as a high-sensitivity detector of neuronal activities. Thus, the method provides a useful tool for studying the activity of astrocytes in brain physiology and pathology.

INTRODUCTION

In neurons, subcellular information collected by dendrites is integrated at the soma to generate all-or-none output signals, that is, the firing of action potentials. Unlike neurons, astrocytes do not produce action potentials. Therefore, information in local subcellular domains, rather than in the soma, may be regarded as the elementary unit for the regulation of cellular processes. The finest astrocyte processes are only tens of nanometers wide, yet they extend throughout brain tissue, where they form close appositions with synapses. It has been suggested that the local intracellular calcium (Ca^{2+}) dynamics of astrocytes regulate gliotransmitter release and modulate neuronal information processing (Haydon and Carmignoto, 2006). We aimed to investigate these activities in astrocytes in the intact brain by developing a highly sensitive in vivo Ca^{2+}-imaging technique.

Previous studies of brain slice preparations have revealed some properties of astrocytic Ca^{2+} dynamics (Di Castro et al., 2011; Panatier et al., 2011; Perea and Araque, 2007; Reeves et al., 2011; Shigetomi et al., 2013a). However, given that astrocytes interact directly with other brain components, including neurons and blood vessels, their physiological functions are best assessed within the intact 3D structure of the brain. Ca^{2+} imaging in astrocytes of the intact brain meets this need (Haydon and Carmignoto, 2006; Iadecola and Nedergaard, 2007).

In the intact brain, Ca^{2+} indicator dyes, such as fluo-4 and Oregon Green BAPTA-1 (OGB1), have been used for in vivo Ca^{2+} imaging after bulk loading of their acetoxymethyl esters. This method stains both neurons and glial cells, making it necessary to perform double labeling with astrocyte-specific sulforhodamine 101 (SR101) to distinguish astrocytes from neurons (Nimmerjahn et al., 2004). One limitation is that the fine processes of astrocytes and Ca^{2+} signals within them cannot be easily visualized. Astrocyte-targeted expression of genetically encoded Ca^{2+} indicators (GECIs) (Mank and Griesbeck, 2008; Pérez Koldenkova and Nagai, 2013) has the potential to overcome these limitations. Previously, a GFP-based intensiometric GECI, membrane-targeted GCaMP3, was used to image near-membrane Ca^{2+} signals in astrocytic processes in brain slices (Shigetomi et al., 2010). Another strategy used a Förster resonance energy transfer (FRET)-based GECI, whereby yellow Cameleon 3.60

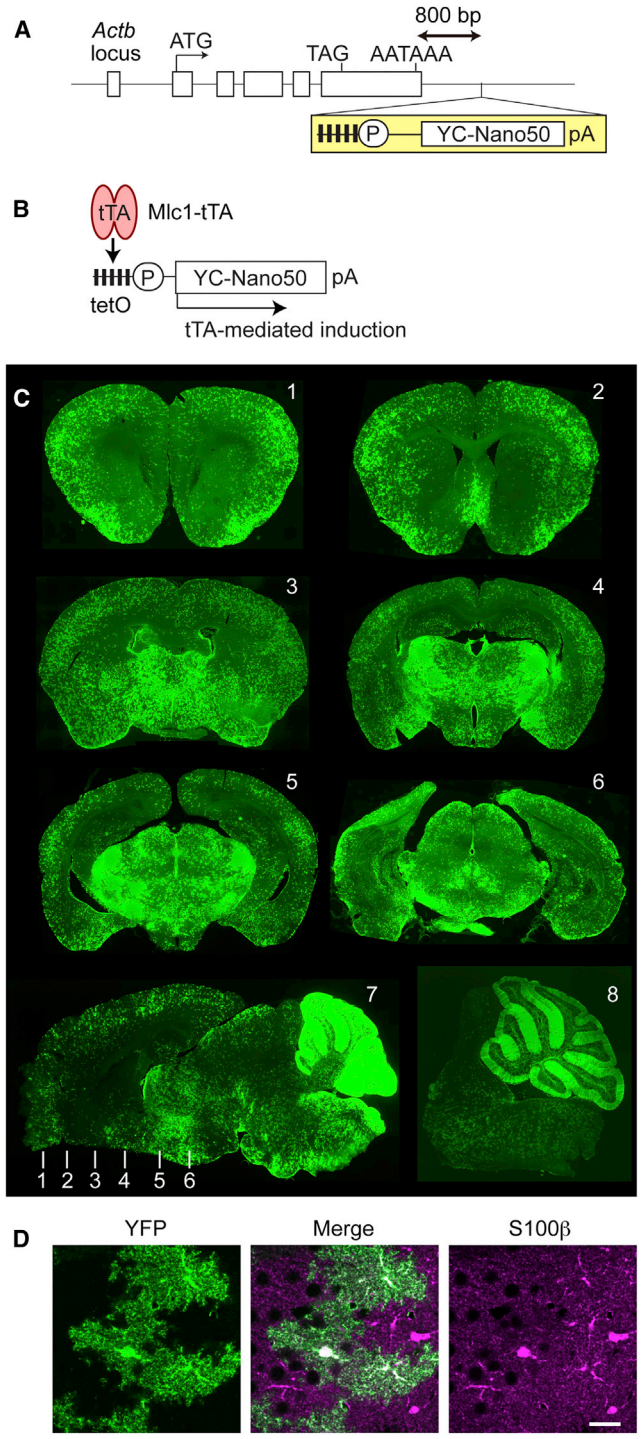

Figure 1. Engineering of Astrocyte-Specific YC-Nano50 Knockin Mice Using KENGE-tet System

(A and B) Strategy for the generation of *Mlc1*-tTA::tetO-YC-Nano50 double-transgenic (Mlc1-YC-Nano50) mice. (A) tetO-YC-Nano50 cassette was inserted 800 bp downstream of the *Actb* polyA signal. (B) Astrocyte-specific YC-Nano50 expression was induced by *Mlc1*-tTA in Mlc1-YC-Nano50 mice.

(C) YC-Nano50 expression patterns in the brain. Coronal (1–6) and sagittal (7 and 8) sections show YFP fluorescence of YC-Nano50. The levels of coronal section were indicated in the sagittal section 7. The highest YC-Nano50 expression was observed in the molecular layer of the cerebellar cortex (section 7 shows saturated YFP signals; section 8 was obtained with a reduced gain of image acquisition). Relatively high expression levels were observed in the ventral portions of the brain including thalamus.

(D) Expression pattern of YC-Nano50 in S100β-positive astrocytes in 4-week-old mice. Representative data obtained from four animals are shown. Scale bar, 20 μm.

See also Figure S1.

(YC3.60) was expressed predominantly in astrocytes and Schwann cells in transgenic mice (Atkin et al., 2009). In vivo imaging of these mice revealed Ca^{2+} signals near the soma of astrocytes; however, Ca^{2+} signals in the fine processes could not be resolved.

Here, we describe a method for high-resolution Ca^{2+} imaging of fine astrocytic processes in living mice. It uses a transgenic mouse line in which a FRET-based GECI, YC-Nano50 (Horikawa et al., 2010), is expressed specifically in astrocytes. By exploiting the ratiometric property of YC-Nano50, we greatly reduce the noise due to motion artifact. The very high Ca^{2+} sensitivity ($K_D \approx 50$ nM) and sufficiently high expression levels of this indicator allowed effective detection of low-amplitude Ca^{2+} signals in astrocytes in vivo.

RESULTS

Generation of Transgenic Mouse Line Expressing YC-Nano50

In order to generate transgenic mice to carry out high-resolution Ca^{2+} imaging in astrocytes in vivo, it is important to select a GECI with an appropriate dynamic range as well as a transgenic method to achieve sufficient levels of expression of the indicator. Based on the range of Ca^{2+} levels between basal and active states in astrocytes, we selected YC-Nano50 as the most suitable YC-Nano variant (Horikawa et al., 2010) (Figures S1A and S1B). To gain selective yet high expression of YC-Nano50, we used the Knockin-mediated ENhanced Gene Expression system, which employs the tetracycline transactivator (tTA)-tet operator (tetO) strategy (KENGE-tet) (Tanaka et al., 2012). We first generated a knockin mouse line in which the tetO-YC-Nano50 cassette was inserted downstream of the β-actin (*Actb*) gene locus (Figure 1A). We then crossed these mice with *Mlc1*-tTA mice in which the expression of tTA is driven by an astrocyte-specific promoter (Tanaka et al., 2010, 2012), resulting in *Mlc1*-tTA::tetO-YC-Nano50 biogenic (Mlc1-YC-Nano50) mice (Figure 1B). Although YC-Nano50 expression in Mlc1-YC-Nano50 mice can be turned off by administration of doxycycline (DOX), we bred the mice without DOX treatment unless otherwise indicated. We observed intensely fluorescent cells with the characteristic morphology of astrocytes in the brain of these mice without the use of immunohistochemical enhancement (Figure 1C), indicating that the expression of YC-Nano50 is abundant and distributed throughout the cytoplasm of the entire cell, including the cell body, trunk, and fine processes. None of the fluorescent cells showed neuronal cell morphology.

To confirm astrocyte-specific expression of YC-Nano50, we performed double immunolabeling of yellow fluorescent protein (YFP) and the following cell-type-specific markers: S100β and

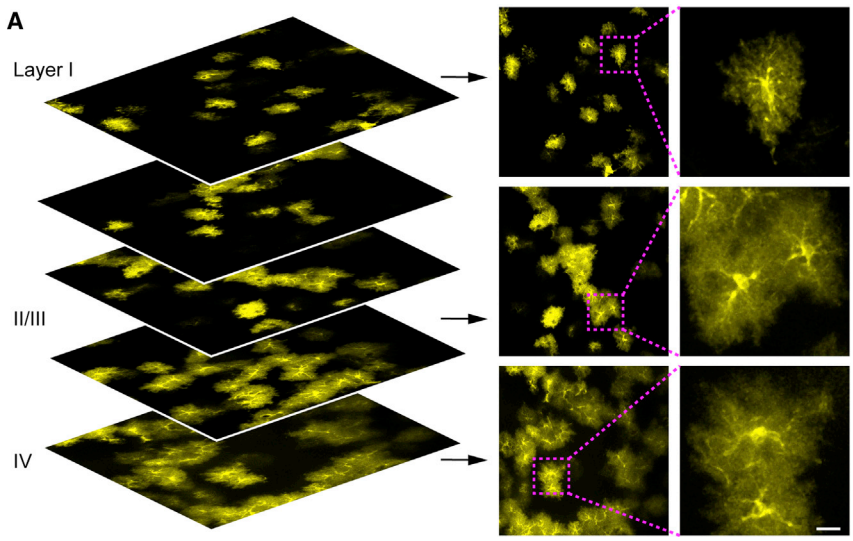

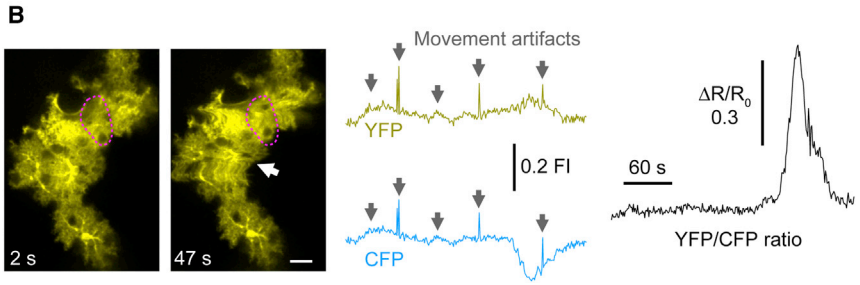

Figure 2. High-Resolution Ca^{2+} Imaging in Astrocytes In Vivo Using YC-Nano50-Expressing Mice

(A) Representative images of YC-Nano50-expressing astrocytes (YFP channel) at different layers of somatosensory cortex of a live Mlc1-YC-Nano50 mouse. Images were acquired in an xyz scan mode using a two-photon microscope. Scale bar, 20 μm. See also Movie S1.

(B) Left: representative time-lapse images of YC-Nano50-expressing astrocytes (YFP channel) in vivo. The white arrow indicates the location where a large motion artifact was observed. Scale bar, 20 μm. Center view shows time courses of the fluorescence intensity change of CFP and YFP within the region of interest indicated by the dotted magenta circle in the left panels. The gray arrows indicate the time points with large motion artifacts. Right view shows isolation of Ca^{2+} signals after obtaining the YFP/CFP ratio.

glial fibrillary acidic protein (GFAP) for astrocytes, NeuN for neurons, Olig2 for adult oligodendrocyte precursor cells, proteolipid protein (PLP) for mature oligodendrocytes, and Iba1 for microglia (Figures 1D and S1C). All YFP-positive cells (n = 151) expressed S100β, and none of YFP-positive cells (n = 102, 120, 138, and 116) expressed other cell-type-specific markers (NeuN, Olig2, PLP, and Iba1) in the somatosensory cortex (Figure S1C). Astrocytes sparsely expressed YC-Nano50: 28% ± 6% and 17% ± 4% of S100β-positive cells expressed YC-Nano50 in the somatosensory cortex and the CA1 hippocampus, respectively. Such a pattern of sparsely distributed but high-expressing cells provides a means to analyze subcellular Ca^{2+} signals within individual astrocytes.

To assess the long-term effect of YC-Nano50 expression, we examined, in 6-month-old mice, whether there are any signs of glial activation as an indicator of toxic effects. We detected no signs of upregulation of GFAP immunoreactivity or activation of microglia in the somatosensory cortex or in the hippocampus (Figures S1D and S1E), indicating that the levels of astrocytic YC-Nano50 expression achieved by our system did not induce toxic effects.

High-Resolution Ca^{2+} Imaging in Astrocytes In Vivo Using YC-Nano50-Expressing Mice

We next used a two-photon microscope to visualize YC-Nano50 expression in the astrocytes of somatosensory cortex of live animals (Figure 2A; Movie S1). Unlike GCaMPs, which have low resting fluorescence, the bright resting yellow fluorescence of YC-Nano50 allowed us to readily identify astrocytes as individual or clusters of cells. In vivo time-lapse imaging of Mlc1-YC-Nano50 mice showed frequent alterations in the fluorescence intensity of both YFP and cyan fluorescent protein (CFP) channels. One source of in-phase fluorescence intensity changes was movement of the brain relative to the objective lens, due to physical activities of the live animal. We found that we could reduce the movement artifacts and extract Ca^{2+} signals by obtaining the YFP/CFP fluorescence intensity ratio (Figure 2B).

We frequently observed spontaneous Ca^{2+} signals in the fine astrocytic processes (Figure 3A; Movie S2). These twinkling Ca^{2+} signals (Ca^{2+} twinkles) were observed as transient but lengthy (over 60 s in duration) (Figure 3B). They occasionally displayed propagating wave-like patterns but were highly localized (~10 μm; see middle-tiled panels in Figure 3A). A summary of Ca^{2+} twinkles revealed preferential occurrences within cell processes (~80%), with rare occurrences in the cell body or trunk. The half-peak duration ($t_{0.5}$) was 41.6 ± 1.6 s (mean ± SEM, n = 269) (shown as Control in Figure 3C).

Astrocytic Ca^{2+} signals require type 2 inositol 1,4,5-trisphosphate receptor (IP_3R2) signaling (Kanemaru et al., 2013; Petravicz et al., 2008; Takata et al., 2011). To investigate whether Ca^{2+} twinkle is generated through the activation of IP_3R2, we produced IP_3R2-deficient Mlc1-YC-Nano50 trigenic (Mlc1-tTA::tetO-YC-Nano50:: *Itpr2*$^{-/-}$) mice. We found that a deficiency in IP_3R2 resulted in a striking reduction in the frequency but only a slight reduction in the peak amplitude and $t_{0.5}$ of individual Ca^{2+} twinkle (shown as IP_3R2KO in Figure 3C; Figure 3D). We observed Ca^{2+} twinkle in IP_3R2KO astrocytes mainly in the fine processes, as was the case with control *Itpr2*$^{+/+}$ astrocytes

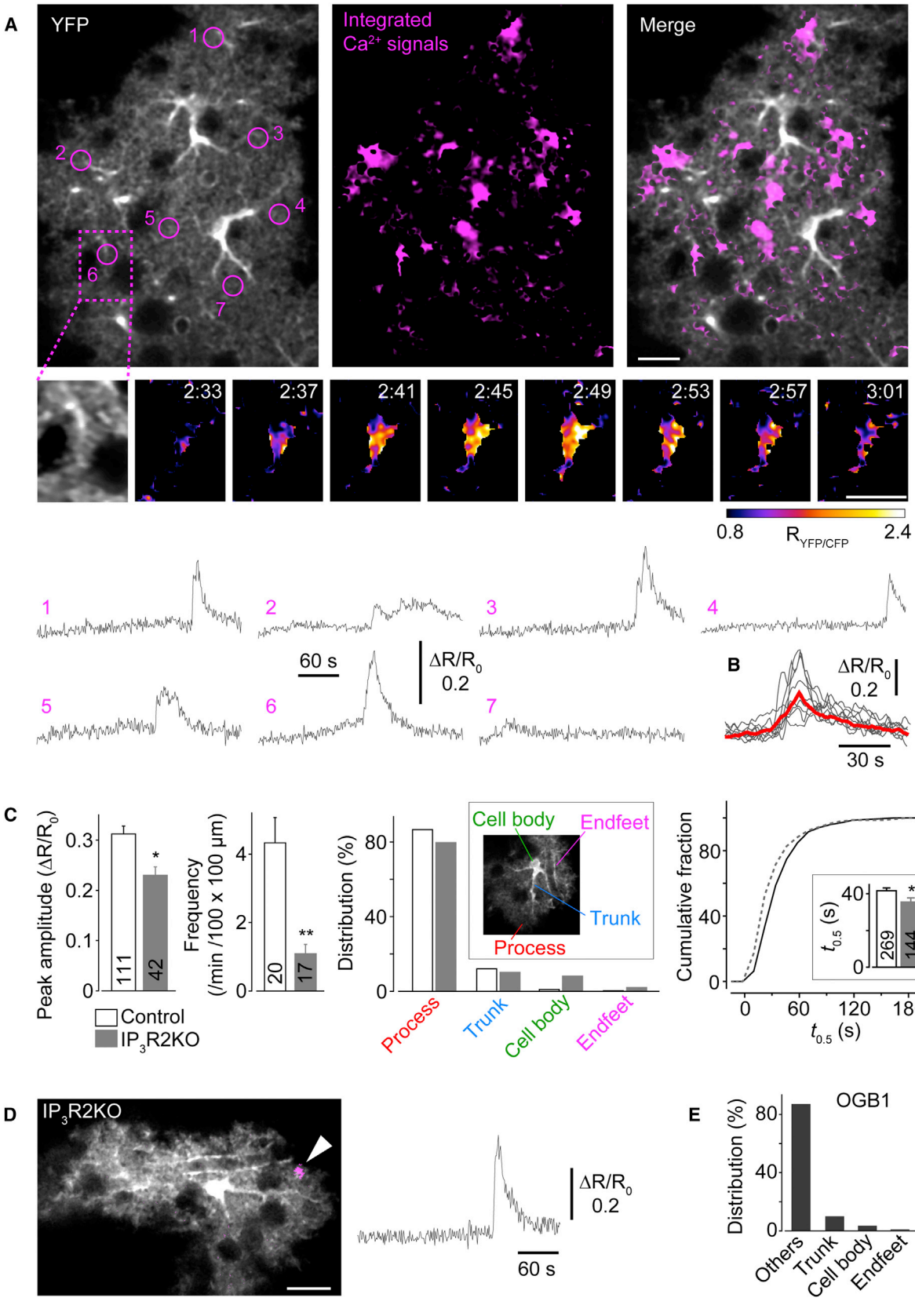

(legend on next page)

(Figures 3C and 3D). These results indicate that although IP_3R2 activity underlies the Ca^{2+} twinkle, other mechanisms are also involved in the generation of the local signals.

We next compared astrocytic Ca^{2+} signals observed in the in vivo studies with those from ex vivo preparations of acute brain slices (Figure S2A; Movie S3). In contrast to Ca^{2+} twinkle observed in vivo, in slice preparations, spontaneous signals in cortical astrocytes frequently occurred in cell bodies, suggesting that within astrocytes, the properties of spontaneous Ca^{2+} signals depend on the condition of the preparation.

We compared whether this method of in vivo Ca^{2+} imaging offers advantages over bulk loading of OGB1. We found that when nontransgenic astrocytes were loaded with OGB1, we could only occasionally observe spontaneous Ca^{2+} signals in the cell bodies or in the trunks of astrocytes (Figures 3E, S2B, and S2C). Most spontaneous Ca^{2+} signals occurred elsewhere, and because with SR101 staining, astrocytic processes can only be traced up to the thickest trunk, we could not determine whether these signals originated from astrocytes, neurons, or nonastrocytic glial cells. Thus, we concluded that the OGB1 method appears to overlook the majority of astrocytic activities.

We next exploited the stable and brain-wide expression of YC-Nano50 in an Mlc1-YC-Nano50 mouse to determine the durability of the Ca^{2+} twinkle signal in astrocytes at different somatosensory cortex locations. Figure S3A shows a representative result of Ca^{2+} twinkle measurements in astrocyte clusters at three different locations within the same mouse. Time-lapse imaging sessions, each lasting for 5 min, were repeated multiple times in each location and then shifted to the next cluster: 24 times at Cluster 1, seven times at Cluster 2, and once at Cluster 3 (Figure S3A). We found that within multiple astrocyte clusters, we could observe stable detection of Ca^{2+} twinkle over a total imaging period of 5 hr. Although the peak amplitude of Ca^{2+} twinkle differed among clusters, we observed no significant difference in the frequency.

Given the high Ca^{2+} affinity of YC-Nano50, it may act as a buffer of intracellular-free Ca^{2+} and therefore interfere with astrocytic Ca^{2+} signals. Exploiting the tet-off system-mediated expression of YC-Nano50 in Mlc1-YC-Nano50 mice, we next examined whether DOX treatment-induced reduction in YC-Nano50 expression levels would affect astrocytic Ca^{2+} signals. During DOX treatment for 10 days, YC-Nano50 expression levels gradually decreased with no effect on the amplitude or on the frequency of Ca^{2+} twinkle (Figures S3B–S3D), suggesting that the expression level of YC-Nano50 in our mouse line does not interfere with Ca^{2+} signaling in astrocytes.

Sensory Stimulation-Evoked Ca^{2+} Signals in Astrocytes of YC-Nano50-Expressing Mice

We then examined the astrocytic response to concerted strong neuronal activity evoked by electrical stimulation of the tail (see Supplemental Experimental Procedures). In the somatosensory cortex of Mlc1-YC-Nano50 mice, we observed large global Ca^{2+} transients within the processes and cell body in response to the stimuli (shown as Control in Figures 4A and 4B). In contrast, the evoked responses were nearly absent in IP_3R2KO astrocytes (shown as IP_3R2KO in Figures 4A and 4B), although these astrocytes displayed Ca^{2+} twinkle (Figures S4A and S4B). We then examined the possible effect of the depth of anesthesia on this result. We did not observe the tail stimulation-evoked Ca^{2+} signals in IP_3R2KO astrocytes even after recovery from anesthesia (Figure S4C). These results indicate that in contrast to Ca^{2+} twinkle, the evoked Ca^{2+} signal propagates throughout the intracellular regions, including the cell body, and is mostly dependent on Ca^{2+} release via IP_3R2.

Close examination of the spatiotemporal properties of the tail stimulation-evoked in vivo astrocytic Ca^{2+} response showed that the fine processes responded prior to the cell body. The Ca^{2+} signal initiated in the fine processes around the peripheral regions and propagated to the cell body at a speed of ~15 μm/s (Figure 4C; Movie S4). These observations show that although somatic Ca^{2+} signals can be evoked by physiological stimuli, the fine astrocytic processes are the initial input sites of the neuron-glia interactions.

Figure 3. Visualization and Characterization of Fine Process-Delimited Spontaneous Ca^{2+} Signal, Ca^{2+} Twinkle

(A) Top: spontaneous Ca^{2+} signals in astrocytic fine processes. In the left panel, astrocytic morphology was determined by the image of the YFP fluorescence. In the center panel, Ca^{2+} signals observed in time-lapse imaging for 5 min are integrated. In the right panel, the two images were overlaid. Middle panel shows time-lapse images of pseudocolored Ca^{2+} signals displaying wave-like propagation within the fine processes. Bottom panels are representative time courses of "twinkling" Ca^{2+} signals observed in the indicated region in the top-left panel. Scale bars, 10 μm. See also Movie S2.

(B) Duration of Ca^{2+} twinkle observed in the imaging field shown in (A). Eight representative traces that had the full time course of both the upstroke and decay phases of Ca^{2+} twinkle were aligned with respect to the peak time (gray), and their averaged trace (red) was superimposed.

(C) Quantification of peak amplitude, frequency, subcellular distribution, and duration ($t_{0.5}$) of Ca^{2+} twinkle in Mlc1-YC-Nano50 mice (shown as Control) and IP_3R2-deficient Mlc1-YC-Nano50 mice (shown as IP_3R2KO). Insets in the distribution and $t_{0.5}$ analyses show the example of morphological criteria and average values of $t_{0.5}$, respectively. The numbers in the bar graphs indicate the number of analyzed events of Ca^{2+} twinkle for peak amplitude, $t_{0.5}$ analyses, and imaging fields (each having a 100 × 100 μm dimension) for frequency analysis. For the distribution analyses, 111 and 42 events of Ca^{2+} twinkle were analyzed in Control and IP_3R2KO, respectively. Data were obtained from four animals. Mean + SEM. *$p = 0.003$ in the peak amplitude analyses; **$p < 0.0005$ in the frequency analyses; $p = 0.025$ in the $t_{0.5}$ analyses, Student's t test. Statistical significance of the difference between the two cumulative histograms ($p = 0.002$) was confirmed using Kolmogorov-Smirnov test.

(D) Spontaneous Ca^{2+} signals in astrocytic fine processes observed in somatosensory cortex in IP_3R2-deficient Mlc1-YC-Nano50 mice. Ca^{2+} signals observed in time-lapse imaging for 5 min are temporally integrated (magenta) and then merged with astrocytic morphology determined by the YFP fluorescence (gray). An arrowhead indicates the site of Ca^{2+} signal, of which time course is shown in the right panel.

(E) Subcellular distribution of spontaneous Ca^{2+} signals visualized by bulk-loaded OGB1 in nontransgenic mice. Note that "Others" may include astrocytic fine processes, nonastrocytic glial cells, and neuropils, which were not stained by SR101. A total of 62 events observed in 20 cells from 2 mice were analyzed. Representative images and traces are shown in Figures S2B and S2C.

See also Figures S2 and S3.

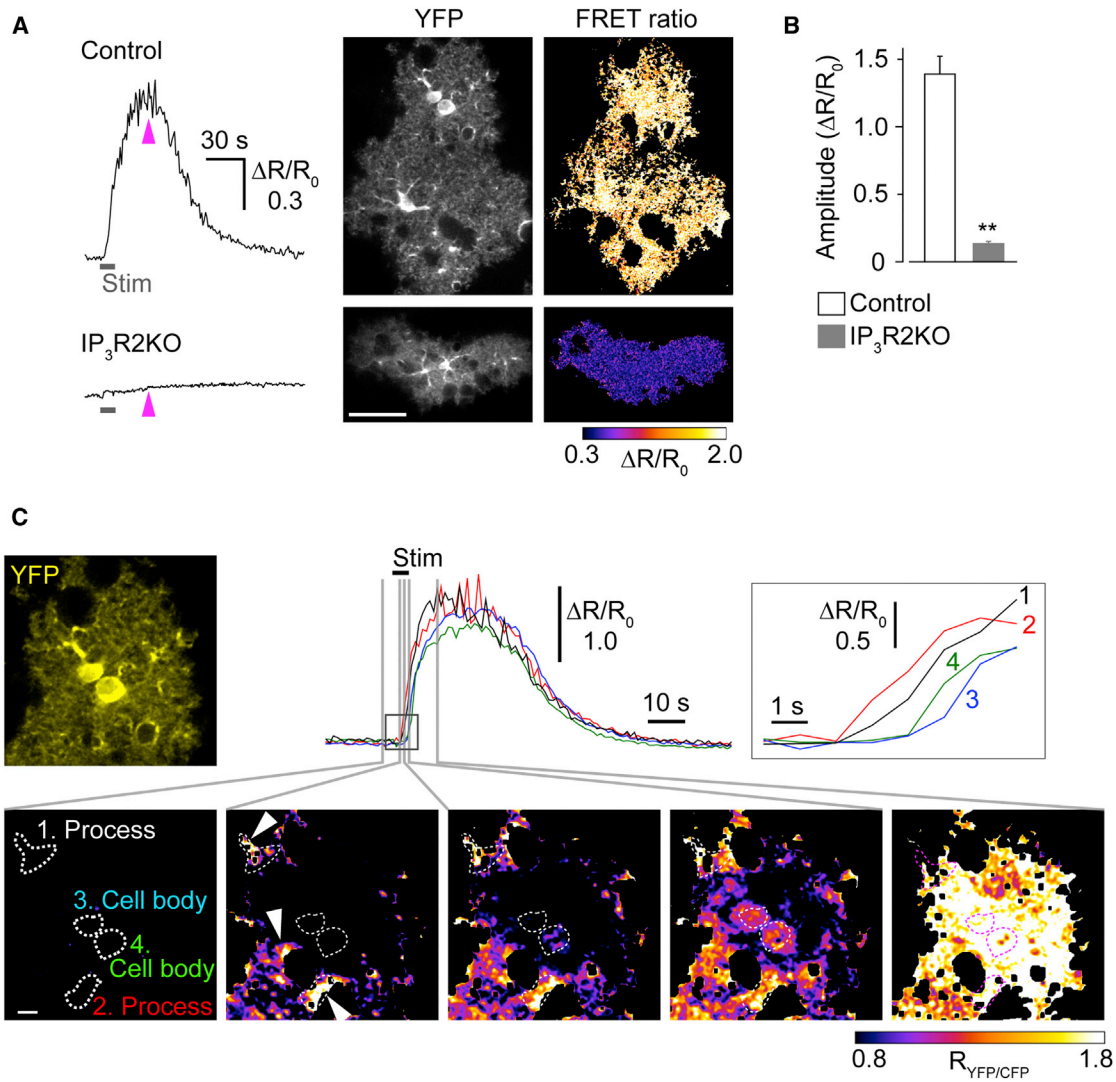

Figure 4. High Sensitivity of Astrocytic Fine Processes to Neuronal Activity

(A) Left: time courses of Ca^{2+} signals within the soma evoked by tail stimulation in transgenic mice. Mlc1-YC-Nano50 is shown in the top as Control, and IP_3R2-deficient Mlc1-YC-Nano50 is shown in the bottom as IP_3R2KO. Right panels show morphology of YC-Nano50-expressing astrocytes (YFP) and pseudocolored Ca^{2+} signal at the time point indicated by the arrowhead in the left traces. Stimulation-evoked Ca^{2+} signals as observed throughout the cells including fine processes in Mlc1-YC-Nano50 mice (see also Movie S4), but not in IP_3R2-deficient Mlc1-YC-Nano50 mice, are shown. Scale bar, 10 μm.

(B) Quantification of the peak amplitude of tail stimulation-evoked Ca^{2+} signals (mean + SEM, Student's t test; n = 42 from 4 Control mice, and n = 23 from 3 IP_3R2KO mice).

(C) Propagation of Ca^{2+} waves evoked by tail stimulation in Mlc1-YC-Nano50 mice. Top-left panel is an image of a YC-Nano50-expressing astrocyte cluster. Top center view shows time courses of Ca^{2+} signals at four locations within the regions of interest shown by dotted lines in the bottom panels. Top-right view shows expanded time courses within the box shown in the top center. Bottom panels are pseudocolor images of evoked Ca^{2+} signals at the time points indicated in the top-center view. Scale bar, 5 μm.

See also Figure S4.

DISCUSSION

In the present study, we developed a tool for the fine visualization of local Ca^{2+} signals in astrocytes in vivo, utilizing the FRET-based GECI, YC-Nano50 (Horikawa et al., 2010). The ratiometric property and ultrahigh sensitivity of YC-Nano50 reduced motion artifacts during in vivo imaging, allowing the detection of low-amplitude Ca^{2+} signals that occur under physiological conditions. YC-Nano50 was expressed in mice using the KENGE-tet system (Tanaka et al., 2012), which drove expression levels of the Ca^{2+} sensor that were sufficient to image the fine processes of astrocytes. Astrocytes in various regions of the brain stably expressed YC-Nano50, enabling us to compare astrocytic activities in different subregions of the brain. Thus, the method is suitable for the in vivo imaging analysis of astrocytic Ca^{2+} signals. The KENGE-tet system can be targeted to the cell type of choice

by selecting different tTA mouse lines, such that the YC-Nano50-based in vivo Ca^{2+}-imaging method can be applied to other cell types.

The high spatiotemporal resolution of the method allowed us to visualize a previously unidentified mode of spontaneous astrocytic Ca^{2+} signals, namely the Ca^{2+} twinkle. Ca^{2+} twinkles are generated in astrocytic fine processes but spread only a short distance within these processes, rarely reaching the cell body. The process-preferential distribution of Ca^{2+} twinkles in vivo (Figure 3C) was not maintained in slice preparations (Figure S2A), indicating that it is a feature of the intact brain, perhaps requiring physiological blood flow and/or intact 3D organization. Local astrocytic Ca^{2+} signals (Ca^{2+} sparkles) were previously observed in Bergmann glial cells in vivo (Nimmerjahn et al., 2009). The duration of sparkles (~10 s) is much shorter than that of the Ca^{2+} twinkles that we have detected (~70 s; Figures 3B and 3C). In addition, due to limitations in resolution, it was not possible to determine conclusively whether individual finer Bergmann glial processes displayed Ca^{2+} sparkles. Therefore, the relationship between Ca^{2+} twinkle in cortical astrocytes and Ca^{2+} sparkles in cerebellar Bergmann glial cells remains to be determined.

IP_3R2 is involved in the generation of Ca^{2+} twinkles, but it is likely that there are also other underlying molecules, which may include Ca^{2+}-permeable ion channels expressed in the plasma membrane (Shigetomi et al., 2012, 2013b). Clarification of these mechanisms will provide clues to understanding the function of Ca^{2+} twinkle, which is currently unknown. In contrast to the Ca^{2+} twinkle, sensory stimulation-induced global Ca^{2+} signals that permeated the cell body, and the generation of these evoked responses, were almost entirely dependent on IP_3R2. These signals originated in the fine processes of the astrocytes and propagated to the cell body, indicating that the fine processes are highly sensitive detectors of neuronal activity. Thus, the method clarifies an important property of astrocytic Ca^{2+} responses in vivo, namely that ongoing astrocytic activity is preferentially displayed in astrocytic fine processes.

Previous reports show the inhibitory effect of anesthetics on astrocytic Ca^{2+} signals (Nimmerjahn et al., 2009; Thrane et al., 2012). It is therefore possible that in our current study, the occurrence of Ca^{2+} twinkle was underestimated due to the use of anesthetized mice, whereby the depth of anesthesia potentially impacted the evoked Ca^{2+} responses. However, we found that in lightly anesthetized mice, the IP_3R2 dependence of tail stimulation-evoked Ca^{2+} signals was maintained. Ca^{2+}-imaging analyses using nonanesthetized mice may clarify these issues.

Further studies using Mlc1-YC-Nano50 mice may help clarify the activities and functions of astrocytes. In addition, through the selection of other tTA mouse lines, subcellular Ca^{2+} signals may be studied in other glial cell types such as oligodendrocytes and microglia. The use of such mice along with pathological mouse models, including neurodegenerative diseases and trauma, will advance the understanding of the contribution of glial cells in brain pathology.

EXPERIMENTAL PROCEDURES

All animal procedures were conducted in accordance with the National Institutes of Health Guide for the Care and Use of Laboratory Animals and approved by the Animal Research Committees of Keio University and The University of Tokyo. Detailed information of entire experimental procedures is available in the Supplemental Experimental Procedures.

For generation of tetO-YC-Nano50 knockin mouse, we utilized a housekeeping gene, *Actb*, for the knockin site (Tanaka et al., 2012) except that the position of gene targeting was 800 bp (as compared with 30 bp in the original method) downstream of the polyA signal. This shift in the targeting site resulted in a decrease in the fraction of astrocytes expressing the transgene (see Figures 1D and S1C). *Mlc1*-tTA (Tanaka et al., 2010, 2012) and IP_3R2 knockout (Li et al., 2005) mice are already published. Genotyping primers are also shown in the Supplemental Experimental Procedures. Standard procedures were taken for immunohistochemistry, and the antibodies used and the reaction times are given in detail in the Supplemental Experimental Procedures.

For in vivo Ca^{2+} imaging, astrocytes in layer II/III of the somatosensory cortex (at a depth of ~300 μm) in craniotomized mice sealed with glass coverslip were imaged. Constant anesthesia level was maintained by a subcutaneous infusion of ketamine, unless otherwise indicated. Imaging was performed using a two-photon laser-scanning microscope, operating at 920 nm (~20 mW under objective), and a water-immersion 25× objective lens. Electric tail stimulation was performed using 30 V pulses with 10 ms duration at a frequency of 20 Hz. A pair of stimulation electrodes separated by 1 cm was placed on the surface of the root of the tail. For the OGB1 imaging, a solution containing OGB1AM and SR101 was injected into the somatosensory cortex.

SUPPLEMENTAL INFORMATION

Supplemental Information includes Supplemental Experimental Procedures, four figures, and four movies and can be found with this article online at http://dx.doi.org/10.1016/j.celrep.2014.05.056.

AUTHOR CONTRIBUTIONS

S.M., H.H., K.H., T.N., and K.F.T. generated gene-targeting animals. K.K., H.S., K.S., N.K., and Y.O. designed and performed imaging analysis. M.X., K.Y., M.M., and K.F.T. performed histological analysis. K.K., K.M., and T.S. performed pilot studies. K.K., T.S., K.M., M.I., and K.F.T. wrote the paper.

ACKNOWLEDGMENTS

We thank Yusuke Kawashima for technical assistance. We thank Yoko Esaki and Saki Nishioka for assistance in the production of the tetO-YC-Nano50 knockin mouse line. This work was supported by grants from Grant-in-Aid for Scientific Research on Innovative Areas "Mesoscopic Neurocircuitry" from the Ministry of Education, Culture, Sports, Science and Technology of Japan (MEXT) (25115729 to K.M.), "Glial Assembly" (25117002 to M.I.), "Brain Environment" (24111551 to K.F.T.), and "Microendophenotype" (25116523 to K.F.T.), Grant-in-Aid for Young Scientists (A) from MEXT (25702054 to K.M.) and (23680042 to K.F.T.), and Takeda Science Foundation (to K.F.T.).

Received: January 17, 2014
Revised: April 16, 2014
Accepted: May 30, 2014
Published: June 26, 2014

REFERENCES

Atkin, S.D., Patel, S., Kocharyan, A., Holtzclaw, L.A., Weerth, S.H., Schram, V., Pickel, J., and Russell, J.T. (2009). Transgenic mice expressing a cameleon fluorescent Ca^{2+} indicator in astrocytes and Schwann cells allow study of glial cell Ca^{2+} signals in situ and in vivo. J. Neurosci. Methods *181*, 212–226.

Di Castro, M.A., Chuquet, J., Liaudet, N., Bhaukaurally, K., Santello, M., Bouvier, D., Tiret, P., and Volterra, A. (2011). Local Ca^{2+} detection and modulation of synaptic release by astrocytes. Nat. Neurosci. *14*, 1276–1284.

Haydon, P.G., and Carmignoto, G. (2006). Astrocyte control of synaptic transmission and neurovascular coupling. Physiol. Rev. *86*, 1009–1031.

Horikawa, K., Yamada, Y., Matsuda, T., Kobayashi, K., Hashimoto, M., Matsuura, T., Miyawaki, A., Michikawa, T., Mikoshiba, K., and Nagai, T. (2010). Spontaneous network activity visualized by ultrasensitive Ca(2+) indicators, yellow Cameleon-Nano. Nat. Methods *7*, 729–732.

Iadecola, C., and Nedergaard, M. (2007). Glial regulation of the cerebral microvasculature. Nat. Neurosci. *10*, 1369–1376.

Kanemaru, K., Kubota, J., Sekiya, H., Hirose, K., Okubo, Y., and Iino, M. (2013). Calcium-dependent N-cadherin up-regulation mediates reactive astrogliosis and neuroprotection after brain injury. Proc. Natl. Acad. Sci. USA *110*, 11612–11617.

Li, X., Zima, A.V., Sheikh, F., Blatter, L.A., and Chen, J. (2005). Endothelin-1-induced arrhythmogenic Ca^{2+} signaling is abolished in atrial myocytes of inositol-1,4,5-trisphosphate(IP_3)-receptor type 2-deficient mice. Circ. Res. *96*, 1274–1281.

Mank, M., and Griesbeck, O. (2008). Genetically encoded calcium indicators. Chem. Rev. *108*, 1550–1564.

Nimmerjahn, A., Kirchhoff, F., Kerr, J.N., and Helmchen, F. (2004). Sulforhodamine 101 as a specific marker of astroglia in the neocortex in vivo. Nat. Methods *1*, 31–37.

Nimmerjahn, A., Mukamel, E.A., and Schnitzer, M.J. (2009). Motor behavior activates Bergmann glial networks. Neuron *62*, 400–412.

Panatier, A., Vallée, J., Haber, M., Murai, K.K., Lacaille, J.C., and Robitaille, R. (2011). Astrocytes are endogenous regulators of basal transmission at central synapses. Cell *146*, 785–798.

Perea, G., and Araque, A. (2007). Astrocytes potentiate transmitter release at single hippocampal synapses. Science *317*, 1083–1086.

Pérez Koldenkova, V., and Nagai, T. (2013). Genetically encoded Ca(2+) indicators: properties and evaluation. Biochim. Biophys. Acta *1833*, 1787–1797.

Petravicz, J., Fiacco, T.A., and McCarthy, K.D. (2008). Loss of IP_3 receptor-dependent Ca^{2+} increases in hippocampal astrocytes does not affect baseline CA1 pyramidal neuron synaptic activity. J. Neurosci. *28*, 4967–4973.

Reeves, A.M., Shigetomi, E., and Khakh, B.S. (2011). Bulk loading of calcium indicator dyes to study astrocyte physiology: key limitations and improvements using morphological maps. J. Neurosci. *31*, 9353–9358.

Shigetomi, E., Kracun, S., Sofroniew, M.V., and Khakh, B.S. (2010). A genetically targeted optical sensor to monitor calcium signals in astrocyte processes. Nat. Neurosci. *13*, 759–766.

Shigetomi, E., Tong, X., Kwan, K.Y., Corey, D.P., and Khakh, B.S. (2012). TRPA1 channels regulate astrocyte resting calcium and inhibitory synapse efficacy through GAT-3. Nat. Neurosci. *15*, 70–80.

Shigetomi, E., Bushong, E.A., Haustein, M.D., Tong, X., Jackson-Weaver, O., Kracun, S., Xu, J., Sofroniew, M.V., Ellisman, M.H., and Khakh, B.S. (2013a). Imaging calcium microdomains within entire astrocyte territories and endfeet with GCaMPs expressed using adeno-associated viruses. J. Gen. Physiol. *141*, 633–647.

Shigetomi, E., Jackson-Weaver, O., Huckstepp, R.T., O'Dell, T.J., and Khakh, B.S. (2013b). TRPA1 channels are regulators of astrocyte basal calcium levels and long-term potentiation via constitutive D-serine release. J. Neurosci. *33*, 10143–10153.

Takata, N., Mishima, T., Hisatsune, C., Nagai, T., Ebisui, E., Mikoshiba, K., and Hirase, H. (2011). Astrocyte calcium signaling transforms cholinergic modulation to cortical plasticity in vivo. J. Neurosci. *31*, 18155–18165.

Tanaka, K.F., Ahmari, S.E., Leonardo, E.D., Richardson-Jones, J.W., Budreck, E.C., Scheiffele, P., Sugio, S., Inamura, N., Ikenaka, K., and Hen, R. (2010). Flexible Accelerated STOP Tetracycline Operator-knockin (FAST): a versatile and efficient new gene modulating system. Biol. Psychiatry *67*, 770–773.

Tanaka, K.F., Matsui, K., Sasaki, T., Sano, H., Sugio, S., Fan, K., Hen, R., Nakai, J., Yanagawa, Y., Hasuwa, H., et al. (2012). Expanding the repertoire of optogenetically targeted cells with an enhanced gene expression system. Cell Reports *2*, 397–406.

Thrane, A.S., Rangroo Thrane, V., Zeppenfeld, D., Lou, N., Xu, Q., Nagelhus, E.A., and Nedergaard, M. (2012). General anesthesia selectively disrupts astrocyte calcium signaling in the awake mouse cortex. Proc. Natl. Acad. Sci. USA *109*, 18974–18979.